Scripta Materialia 146 (2018) 295–299

Contents lists available at ScienceDirect

Scripta Materialia

journal homepage: www.elsevier.com/locate/scriptamat

Regular article

Thermoelectric properties and cost optimization of spark plasma sintered *n*-type $Si_{0.9}Ge_{0.1}$ - Mg_2Si nanocomposites

Andrey Usenko [a,*], Dmitry Moskovskikh [a], Andrey Korotitskiy [a], Mikhail Gorshenkov [a], Elena Zakharova [a], Aleksandr Fedorov [b,c], Yury Parkhomenko [a], Vladimir Khovaylo [a,d]

[a] National University of Science and Technology "MISiS", Moscow 119049, Russia
[b] Siberian Federal University, Krasnoyarsk 660041, Russia
[c] Kirensky Institute of Physics, Krasnoyarsk 660036, Russia
[d] National Research South Ural State University, Chelyabinsk 454080, Russia

ARTICLE INFO

Article history:
Received 14 November 2017
Accepted 15 December 2017
Available online 21 December 2017

Keywords:
Thermoelectric materials
Spark plasma sintering
Mechanical alloying
Silicon
Germanium
Magnesium silicide
Nanocomposite

ABSTRACT

We report on thermoelectric properties of low Ge content *n*-type $Si_{0.9}Ge_{0.1}$–Mg_2Si nanocomposite. Introduction of the Mg_2Si phase into a SiGe matrix resulted in a dramatic drop of the lattice thermal conductivity beyond the previously reported lowest limit for SiGe alloys due to intensification of phonon scattering on SiGe–Mg_2Si grain boundaries. For a sample doped with 1 at.% of Mg_2Si, the peak value of thermoelectric figure of merit *ZT* reached ~0.8 at 800 °C. Sintered nanocomposites still exhibit high thermoelectric performance while being almost two times cheaper than $Si_{0.8}Ge_{0.2}$.

It is well known that thermoelectric (TE) materials such as silicon germanium alloys have been used in radioisotope thermoelectric generators (RTG) for NASA space missions [1]. High mechanical strength and resistance to atmospheric oxidation make this material suitable for a number of practical applications [1,2]. It has been demonstrated that SiGe alloys can be effectively used as a high temperature stage for cascade thermoelectric generators and less effectively in segmented generators due to their low compatibility factor [3–5]. Thermoelectric efficiency of any material is determined by dimensionless figure of merit, $ZT = \frac{\alpha^2 \sigma T}{k}$, where *S* is Seebeck coefficient, σ is electrical conductivity and *k* is thermal conductivity [1]. Resent progress in increasing *ZT* has been mainly driven by a reduction of thermal conductivity via nanostructuring approach [6–14]. It has been demonstrated that thermal and electrical transport is influenced by crystallite boundary scattering. If the crystallite sizes in a nanostructured material are comparable with the phonon mean free path but are larger than the charge carrier mean free path, thermal conductivity is reduced more significantly than the electrical conductivity and this finally results in enhancement of *ZT* value. By employing a similar approach, the authors have earlier reported a high value of $ZT = 1.05$ for *n*-type nanostructured SiGe alloys by using spark plasma sintering of mechanically alloyed fine powders [15].

Multiphase composite materials have been also considered for thermoelectric applications. In 1999 Bergman and Fel have showed that composite material structures can improve the power factor over the constituent components [16]. Later Mingo et al. [17] have performed electron and phonon transport calculations for nanocomposites consisting of silicide nanoparticles embedded in a SiGe matrix. They confirmed the previous studies that the thermal conductivity can be decreased beyond the solid solution limit [18] via nanostructuring of the SiGe alloys to enhance ZT. Furthermore, they discussed that silicide nanoinclusions can improve TE power factor of nanocomposites through preferential scattering of the low energy charge carriers. Experimental investigations have been performed for SiGe-based nanocomposites with the addition of $FeSi_2$, $CrSi_2$, $MoSi_2$, and WSi_2 [19–23]. Previous results have showed that a significant reduction of thermal conductivity is possible in silicide–SiGe nanocomposites as compared to polycrystalline or nanostructured SiGe. The most significant boost of thermoelectric performance has been reported by Ahmad et al. [24] for *p*-type SiGe–YSi_2 with *ZT* ~1.81 at 827 °C, which is ~34% higher as compared to reported earlier the best values for *p*-type nanostructured SiGe. The authors have explained such dramatic growth of *ZT* as due to the formation of a network of the coherent grain boundaries at nanoscale in SiGe–YSi_2 by engineering at atomic scale. The coherent

* Corresponding author.
E-mail address: usenko@misis.ru (A. Usenko).

https://doi.org/10.1016/j.scriptamat.2017.12.019
1359-6462/

Table 1
Sintering parameters and volume density of *n*-type $Si_{0.9}Ge_{0.1}$–Mg_2Si nanocomposites.

Sample	Sintering temperature, °C	Soaking time, min	Pressure, MPa	Heating rate, °C/min	Density, % of theoretical
$Si_{0.9}Ge_{0.1}$	1150	5	65	75	98.81
$Si_{0.9}Ge_{0.1}$–Mg_2Si 1% (at.)	1100	5	65	75	98.53
$Si_{0.9}Ge_{0.1}$–Mg_2Si 3% (at.)	1065	5	65	75	95.12
$Si_{0.9}Ge_{0.1}$–Mg_2Si 10% (at.)	1045	5	65	75	93.97

boundaries effectively scatter phonons but allow charge carriers to pass through.

Recently, Nozariasbmarz et al. have reported on the very promising $ZT = 1.3$ at 900 °C for *n*-type SiGe–Mg_2Si utilizing a smaller amount of germanium as compared to the RTG SiGe [25]. This would definitely be a significant achievement in the development of high temperature thermoelectric converters with a lower cost and a higher efficiency. However, it must be noted that dependence of *ZT* on sintering parameters as well as on the Mg_2Si content in SiGe–Mg_2Si nanocomposites has not been studied in Ref. [25]. Moreover, reported by Nozariasbmarz et al. sintering temperature $T = 1250$ °C of the studied SiGe–Mg_2Si nanocomposite is very peculiar in the sense that it is almost 150 °C higher than the melting temperature of Mg_2Si. Generally, the liquid phase sintering technique is very complicated, especially in the case of nanocomposites, because the high internal stresses which can be generated by the melting of one of the nanocomposites' component usually lead to the wrecking of the molding tools. The mentioned above concerns and a high demand for the development of low cost – high efficiency thermoelectric materials motivated us to an extended investigation of SiGe–Mg_2Si nanocomposites.

In this paper, *n*-type $Si_{0.9}Ge_{0.1}$–Mg_2Si nanocomposites were investigated with respect to the Mg_2Si doping level and the results obtained were compared with the previously studied nanostructured *n*-type $Si_{0.8}Ge_{0.2}$ alloys [6]. The Ge content was decreased compared to conventional $Si_{0.8}Ge_{0.2}$ alloys in order to reduce the materials cost, since it was expected the lattice thermal conductivity of nanocomposite k_L would be rather low despite the fact that k_L of crystalline $Si_{0.9}Ge_{0.1}$ is almost two times higher [18,26].

The raw chemical element Si, Ge, P of at least 99.99% purity and Mg_2Si powder (Alfa Aesar) of 99.5% purity were used for preparation of the samples. First, Si, Ge and P were mixed in desired proportions and ball milled in Fritsch 5 Pulverisette ball mill by using reference parameters [7]. Then nanopowders of SiGe solid solution and Mg_2Si (~20 mesh) powder were mixed in desired proportions and then ball milled in Frisch 7 Pulverisette ball mill. The vial of the ball mill and the milling media were made of zirconium oxide. The ball-to-powder weight ratio was 20:1 and the process was carried out in an argon atmosphere at a speed of 700 rpm. 1 wt% of anti-friction and re-welding control agent (alcohol) was added to the vials. The samples were sintered from the powder using spark plasma sintering (SPS) technique (Labox 650, Sinter Land, Japan). The powders were put into a cylindrical graphite die which was placed in a camera evacuated to a high vacuum. Uniaxial pressure was then applied through top and bottom plungers. Each plunger has a diameter of 12.7 mm and a length of 23 mm. The composite samples were prepared using the following sintering conditions: the samples were compressed at room temperature for 1 min, then the pressure was risen up to 60 MPa; temperature of the samples was gradually raised to 1045–1100 °C depending on Mg_2Si content in the samples with a heating rate of 75 °C/min; after the soaking time of 5 min, the pressure was reduced to 10 MPa and the samples were cooled. Experimental parameters of temperature, applied pressure, current, voltage, and sample displacement were recorded simultaneously. Temperature was recorded by a thermocouple (Type R) inserted in a hole drilled into the die surface to a depth of 3.5 mm. The compacted disc samples have a dimension of 12.7 mm (diameter) × 2 mm (height). The samples were annealed at 900 °C during one week. Microstructure of the samples was examined by scanning electron microscopy. Elemental composition was analyzed by Energy Dispersive Spectroscopy (EDS). Studies of the phase composition were carried out by Dron-2 X-ray diffractometer (Russia) at room temperature using Co-K_α radiation ($\lambda = 1.79026$ Å). Density of the samples was determined by the Archimedes technique. Thermal conductivity measurements were carried out using a laser flash analysis system (Netzsch LFA 457) from room temperature up to 900 °C. Specific heat was measured by a differential scanning calorimeter (DSC) Netzsch 204 F1. Electrical conductivity and Seebeck coefficient were measured simultaneously on bars measuring $1 \times 3 \times 12$ mm^3 using a homemade transport measuring system (Cryotel Ltd.) up to 800 °C. The accuracy of these measurements was checked against a silver sample of 99.99% purity.

Table 1 summarizes the sintering parameters and volume density of *n*-type $Si_{0.9}Ge_{0.1}$ and $Si_{0.9}Ge_{0.1}$–Mg_2Si specimens. Sintering temperature of the nanocomposites was chosen with respect to Mg_2Si melting point –. Samples presented in this work were synthesized at temperatures below the melting temperature of Mg_2Si $T_m = 1102$ °C. However there were numerous attempts to synthesized nanocomposites by the so called liquid phase sintering technique (LPS) [27] to achieve higher values of volume density. These attempts were unsuccessful more likely due to poor wetting because of high values of contact angle between sintering components Even, below the melting temperature of Mg_2Si we faced with a local overheating due to SPS process that induced a local liquid phase formation and thereby led to high internal stresses that broke the samples. Thus the sintering temperature was decreased from 1100 °C to 1045 °C as the Mg_2Si content increased from 1% to 10% (Table 1). Fig. 1 shows XRD patterns of *n*-type $Si_{0.9}Ge_{0.1}$–Mg_2Si 10% (at.) specimen: (a) mechanically alloyed SiGe nanopowder and Mg_2Si nanopowder mixture, (b) spark plasma sintered, (c) annealed at 900 °C. It is apparent from the figure that Ge completely dissolves in Si matrix after 2 h of ball milling and Mg_2Si is maintained after the ball milling. The XRD peaks exhibit significant broadening because of the size effect and considerable amount of strains in nanopowder due to impact of shear forces of milling media during the high energy ball milling.

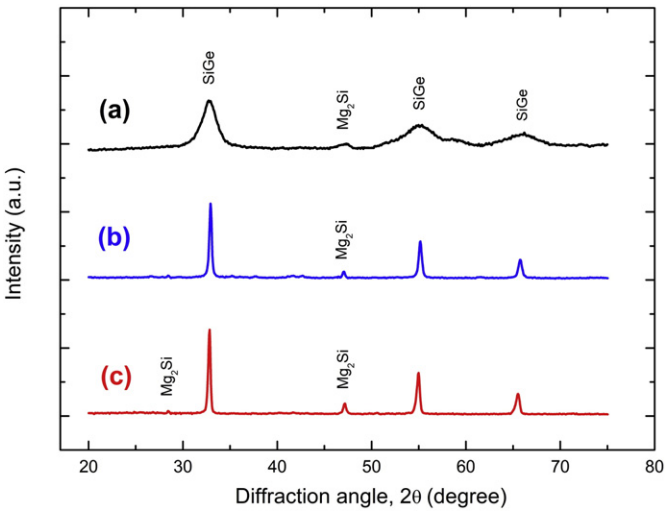

Fig. 1. XRD patterns collected for *n*-type $Si_{0.9}Ge_{0.1}$–Mg_2Si 10% (at.): a) powder, b) spark plasma sintered and c) annealed sample.

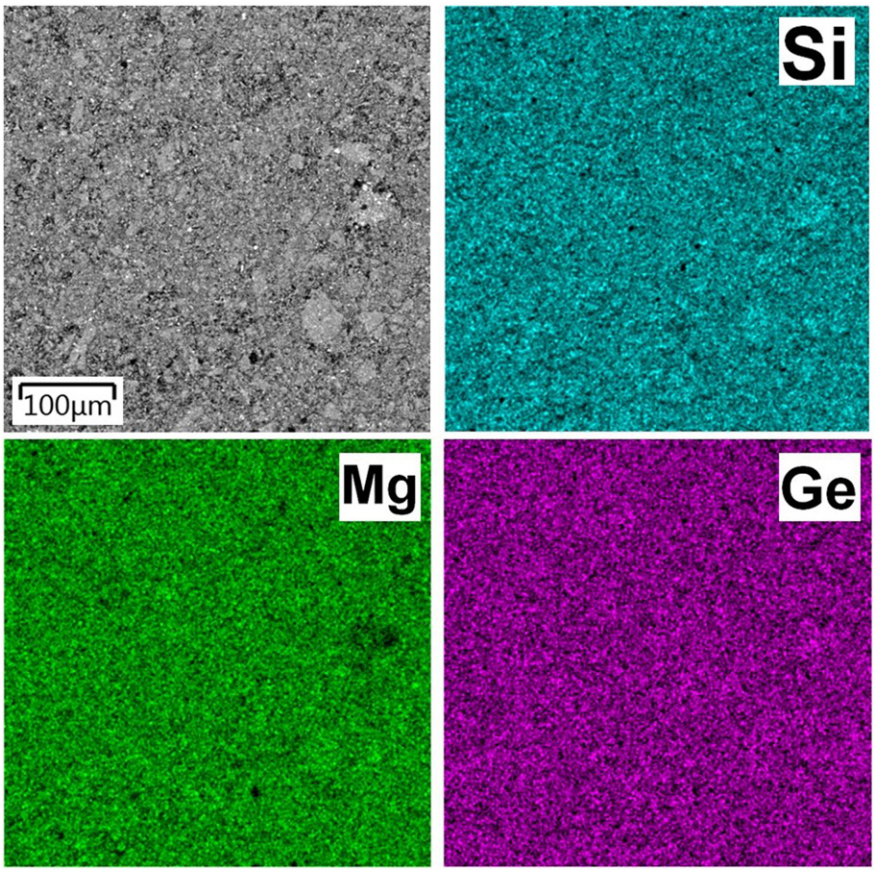

Fig. 2. SEM image and EDS elemental mapping of Si, Mg and Ge of bulk $Si_{0.9}Ge_{0.1}$–Mg_2Si 10% (at.) nanocomposite after annealing.

The possibility of retained nanograins for sintering temperature up to 1150 °C was previously demonstrated for bulk nanostructured $Si_{0.8}Ge_{0.2}$ alloys [6,7,15]. Thus the growth of peak intensity is mainly attributed to the lattice strain sharp fall after SPS and subsequent annealing [28]. The elemental mapping of $Si_{0.9}Ge_{0.1}$–Mg_2Si 10% (at.) presented in Fig. 2 confirms overall chemical homogeneity of the nanocomposite.

The main advantage of using SiGe nanostructuring approach for ZT enhancement is attributed to the fact that there is a large difference between mean free path of electrons and phonons: approximately 5 nm for electrons and 2–300 for phonons in highly doped samples at 25 °C [14]. Thus any nanostructure can reduce the phonon thermal conductivity without significant penalty for the electrical conductivity. Introducing Mg_2Si phase into SiGe matrix resulted in dramatic drop of lattice thermal conductivity that overcome the previous lowest limit for SiGe alloys due to intensification of phonon scattering on SiGe–Mg_2Si grain boundaries [19]. Fig. 3a clearly shows that the prepared nanocomposites demonstrated a sharp drop of thermal conductivity as compared to the bulk RTG sample [1] and previously studied nanostructured *n*-type $Si_{0.8}Ge_{0.2}$ alloy [6]. The achieved values of thermal conductivity 1.5–2.5 $Wm^{-1}\ K^{-1}$ are lower than those reported by Wang et al. [14], Bathula et al. [15] and Nozariasbmarz et al. [25]. The drop of thermal conductivity was driven by: 1) intensification of phonon scattering on grain boundaries and 2) a decrease of the volume density of the sintered samples with the increase of Mg_2Si content.

For further understanding of behavior of the thermal conductivity, the contributions from the lattice thermal conductivity and from the electronic thermal conductivity were separated. The total thermal conductivity is given by $k_{total} = k_e + k_L$ where k_e and k_L are the contributions to the thermal conductivity from the carriers and the lattice, respectively. We calculate the electronic thermal conductivity using the Wiedemann-Franz law $k_e/\sigma = LT$, where L – Lorenz number. The lattice thermal conductivity was defined as the difference between

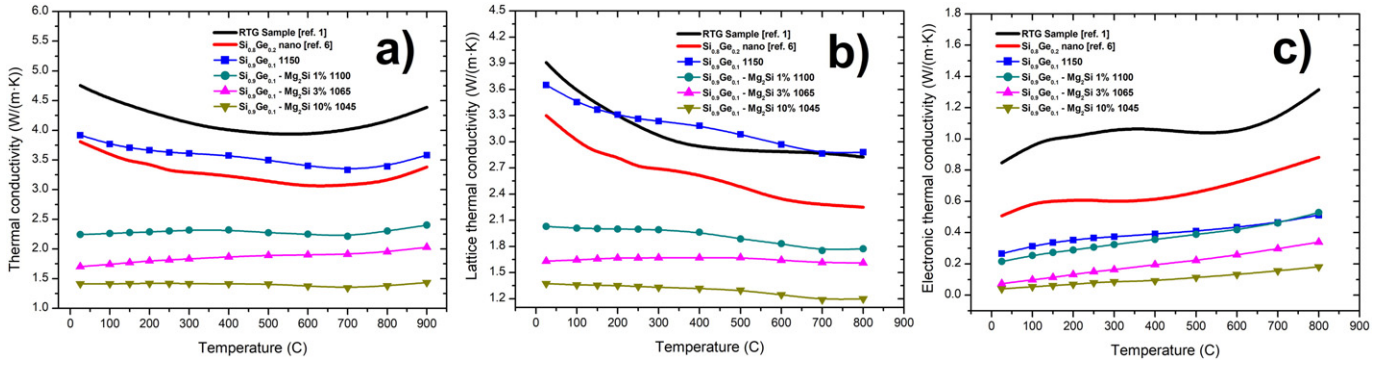

Fig. 3. Total (a), electronic (b) and lattice (c) thermal conductivities of sintered $Si_{0.9}Ge_{0.1}$–Mg_2Si nanocomposites, reference RTG sample [1] and bulk nanostructured $Si_{0.8}Ge_{0.2}$ sample [6].

total and electronic thermal conductivity. Sintered nanocomposites demonstrated a linear behavior of the electronic thermal conductivity (Fig. 3b) which somewhat differs from that reported for the reference SiGe samples [1,6]. As far as the reference samples are highly doped degenerate semiconductors the curve shape demonstrated a non-monotonic behavior which is changed to linear at high temperatures due to an increase of the intrinsic carrier concentration. The electronic contribution to the total thermal conductivity correlated with the electrical conductivity and its influence on the total thermal conductivity is rather weak. Fig. 3c shows the significant drop of lattice thermal conductivity down to 1.4 $Wm^{-1} K^{-1}$ for $Si_{0.9}Ge_{0.1}$–Mg_2Si 10% (at.) sample which indicates that the effect of grain boundaries scattering in nanocomposite can compensate the lack of Ge in the SiGe matrix. The lattice thermal conductivity reduced with the temperature due to enhancement of phonon-phonon scattering.

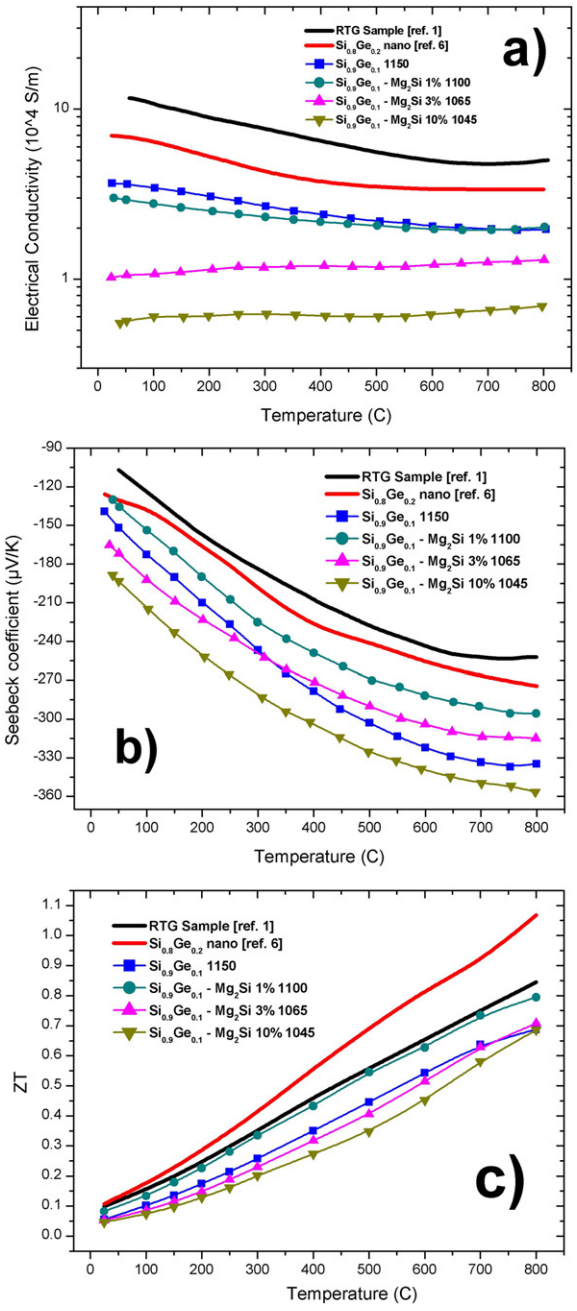

Fig. 4. Temperature dependence of the electrical conductivity (a), Seebeck coefficient (b) and ZT (c) of sintered $Si_{0.9}Ge_{0.1}$–Mg_2Si nanocomposites, reference RTG sample [1] and bulk nanostructured $Si_{0.8}Ge_{0.2}$ sample [6].

Fig. 4a shows temperature-dependent electrical conductivity. The electrical conductivity values are strongly influenced by the chemical composition and the sintering temperature. The behavior of the electrical conductivity is typical for highly doped semiconductors for $Si_{0.9}Ge_{0.1}$ 1150 sample and $Si_{0.9}Ge_{0.1}$–Mg_2Si 1% (at.). In contrast, $Si_{0.9}Ge_{0.1}$–Mg_2Si 3% (at.) and $Si_{0.9}Ge_{0.1}$–Mg_2Si 10% (at.) specimens demonstrated nearly monotonic growth of the electrical conductivity that is relevant for non-degenerate semiconductors. As it seen from Fig. 4a and Fig. 3a the electrical conductivity is decreasing faster than the thermal conductivity with the decreasing sintering temperature for the samples sintered at 1065 °C and 1045 °C. Thus the electrical conductivity of $Si_{0.9}Ge_{0.1}$–Mg_2Si 10% (at.) dropped to 0.6 10^4 $Sm \cdot m^{-1}$. The Seebeck coefficient absolute values presented in Fig. 4b demonstrated significant growth for all nanocomposite samples with the increase of Mg_2Si content. This is more likely due to lower carrier concentration in nanocomposite samples which also explains rather low values if the electrical conductivity. The ZT value of *n*-type $Si_{0.9}Ge_{0.1}$–Mg_2Si nanocomposites follows the similar trend as that of RTG and previously studied nanostructured sample (Fig. 4c). Although the thermal conductivity of the studied nanocomposites decreased dramatically, ZT remains almost equal to that of the RTG sample due to simultaneous decrease of the power factor driven by fall of the electrical conductivity.

The thermoelectric properties of *n*-type $Si_{0.9}Ge_{0.1}$–Mg_2Si nanocomposites were studied in the temperature range from 25 to 800 °C. Sintered nanocomposites demonstrated significant decrease of the thermal conductivity down to 1.5–2.5 $Wm^{-1} K^{-1}$. The result can be explained by the interface scattering mechanism for mid- to long-wavelength phonons, resulting in a further reducing thermal conductivity that is lower than the alloy limit. The maximum ZT value reaches 0.8 at 800 °C for $Si_{0.9}Ge_{0.1}$–Mg_2Si 1% (at.), which is almost equal to RTG sample. This study highlights that the nanocomposites with low Ge content could have competitive ZT values as well as being cost effective. In order to enhance the ZT of current $Si_{0.9}Ge_{0.1}$–Mg_2Si nanocomposites new sintering solution required to achieve higher dense structures to maintain high values of the power factor.

This work was supported by Russian Science Foundation (project No. 16-13-00060). Part of the work (structural characterization of the samples) was carried out with financial support of the Ministry of Education and Science of the Russian Federation in the framework of Increase Competitiveness Program of NUST "MISiS". Partial support by Act 211 Government of the Russian Federation, contract # 02.A03.21.0011, is also acknowledged.

References

[1] D.M. Rowe, Thermoelectrics Handbook: Macro to Nano, 80, CRC Press, 2005.
[2] T. Hendricks, W.T. Choate, Engineering Scoping Study of Thermoelectric Generator Systems for Industrial Waste Heat Recovery, 20, US Dep. Energy, 2006 74.
[3] Z. Ouyang, D. Li, Sci. Rep. 6 (2016) 24123.
[4] G.J. Snyder, Appl. Phys. Lett. 84 (2004) 2436–2438.
[5] M.S. El-Genk, H.H. Saber, AIP Conf. Proc. 699 (2004) 230.
[6] A.A. Usenko, D.O. Moskovskikh, M.V. Gorshenkov, A.V. Korotitskiy, S.D. Kaloshkin, A.I. Voronin, V.V. Khovaylo, Scr. Mater. 96 (2015) 9–12.
[7] A. Usenko, D. Moskovskikh, M. Gorshenkov, A. Voronin, A. Stepashkin, S. Kaloshkin, D. Arkhipov, V. Khovaylo, Scr. Mater. 127 (2017) 63–67.
[8] P. Bellanger, S. Gorsse, G. Bernard-Granger, C. Navone, A. Redjaimia, S. Vivès, Acta Mater. 95 (2015) 102–110.
[9] D.B. Xiong, N.L. Okamoto, H. Inui, Scr. Mater. 69 (2013) 397–400.
[10] L.P. Bulat, V.B. Osvenskii, D.A. Pshenay-Severin, Mater. Today Proc. 2 (2015) 532–537.
[11] D. Berthebaud, T. Nishimura, T. Mori, J. Mater. Res. 25 (2010) 665–669.
[12] A.T. Burkov, S.V. Novikov, V.V. Khovaylo, J. Schumann, J. Alloys Compd. 691 (2017) 89–94.
[13] C. Bera, M. Soulier, C. Navone, G. Roux, J. Simon, S. Volz, N. Mingo, J. Appl. Phys. 108 (2010) 124306.
[14] X.W. Wang, H. Lee, Y.C. Lan, G.H. Zhu, G. Joshi, D.Z. Wang, J. Yang, A.J. Muto, M.Y. Tang, J. Klatsky, S. Song, M.S. Dresselhaus, G. Chen, Z.F. Ren, Appl. Phys. Lett. 93 (2008) 193121.
[15] S. Bathula, M. Jayasimhadri, N. Singh, A.K. Srivastava, J. Pulikkotil, A. Dhar, R.C. Budhani, Appl. Phys. Lett. 101 (2012) 213902.
[16] D.J. Bergman, L.G. Fel, J. Appl. Phys. 85 (1999) 8205–8216.

[17] N. Mingo, D. Hauser, N.P. Kobayashi, M. Plissonnier, A. Shakouri, Nano Lett. 9 (2009) 711–715.
[18] E.R. Johnson, S.M. Christian, Phys. Rev. 95 (1954) 560–561.
[19] Z. Zamanipour, D. Vashaee, J. Appl. Phys. 112 (2012) 1–9.
[20] P. Rouhani, Z. Zamanipour, J.S. Krasinski, D. Vashaee, L. Tayebi, 2012 IEEE Green Technol. Conf. 2012 1–4.
[21] A. Usenko, D. Moskovskikh, A. Korotitskiy, M. Gorshenkov, A. Voronin, D. Arkhipov, M. Lyange, G. Isachenko, V. Khovaylo, J. Electron. Mater. 45 (2016) 3427–3432.
[22] F.W. Dynys, A. Sayir, J. Mackey, A. Sehirlioglu, J. Alloys Compd. 604 (2014) 196–203.
[23] K. Favier, G. Bernard-Granger, C. Navone, M. Soulier, M. Boidot, J. Leforestier, J. Simon, J.C. Tedenac, D. Ravot, Acta Mater. 64 (2014) 429–442.
[24] S. Ahmad, A. Singh, A. Bohra, R. Basu, S. Bhattacharya, R. Bhatt, K.N. Meshram, M. Roy, S.K. Sarkar, Y. Hayakawa, A.K. Debnath, D.K. Aswal, S.K. Gupta, Nano Energy 27 (2016) 282–297.
[25] A. Nozariasbmarz, P. Roy, Z. Zamanipour, J.H. Dycus, M.J. Cabral, J.M. LeBeau, J.S. Krasinski, D. Vashaee, APL Mater. 4 (2016) 104814.
[26] J. Garg, N. Bonini, B. Kozinsky, N. Marzari, Phys. Rev. Lett. 106 (2011) 45901.
[27] R.M. German, Liquid Phase Sintering, Springer Science & Business Media, 2013.
[28] S. Bathula, M. Jayasimhadri, B. Gahtori, N.K. Singh, K. Tyagi, A.K. Srivastava, A. Dhar, Nano 7 (2015) 12474–12483.